Received 25 February 2022; accepted 17 March 2022. Date of publication 21 March 2022; date of current version 28 March 2022.

Digital Object Identifier 10.1109/OJCOMS.2022.3160721

Reduced-Complexity FFT-Spread Multicarrier Faster-Than-Nyquist Signaling in Frequency-Selective Fading Channel

TAKUMI ISHIHARA (Member, IEEE), AND SHINYA SUGIURA (Senior Member, IEEE)

Institute of Industrial Science, The University of Tokyo, Tokyo 153-8505, Japan

CORRESPONDING AUTHOR: S. SUGIURA (e-mail: sugiura@ieee.org)

The work of Takumi Ishihara was supported in part by the Japan Society for the Promotion of Science (JSPS) KAKENHI under Grant 20K22410. The work of Shinya Sugiura was supported in part by the Japan Science and Technology Agency (JST) Precursory Research for Embryonic Science and Technology (PRESTO) under Grant JPMJPR1933. Part of this paper was accepted for presentation at IEEE ICC2022.

ABSTRACT In this paper, we propose novel reduced-complexity fast Fourier transform (FFT)-spread multicarrier faster-than-Nyquist (MFTN) signaling with power allocation for a frequency-selective fading channel. The information rate of the proposed MFTN signaling is derived by relying on the circulant approximation of the FTN-specific intersymbol interference matrix and noise covariance matrix. This allows us to constitute efficient calculations of precoding and weighting matrices. The power allocation coefficients are optimized such that the approximated information rate is maximized. Our simulation results demonstrate that the proposed scheme with power allocation achieves the bit error ratio (BER) performance close to the conventional eigenvalue-decomposition (EVD)-precoded FTN signaling counterpart that is optimal in terms of an achievable information rate while significantly reducing the computational complexity as low as the order of $\mathcal{O}(N \log N)$. While the proposed scheme exhibits a high peak-to-average-power ratio similar to the conventional EVD-precoded counterpart due to the effects of FFT-based precoding, it achieves better BER performance than the conventional open-loop single-carrier FTN signaling scheme and the Nyquist signaling scheme, employing the same root-raised cosine shaping filter. It is also confirmed that the proposed MFTN signaling scheme does not suffer from any significant bandwidth broadening.

INDEX TERMS Cyclic prefix, eigenvalue decomposition, faster-than-Nyquist signaling, fast Fourier transform, frequency-selective channel, low-complexity detection, Nyquist criterion, power allocation.

I. INTRODUCTION

CONVENTIONAL wireless communication systems are designed based on the Nyquist criterion that enables intersymbol interference (ISI)-free orthogonal data transmission in the time domain. The Nyquist criterion defines a minimum symbol interval by $T_0 = 1/(2W)$, where $2W$ represents the bandwidth of an ideal rectangular shaping filter, and the associated maximum symbol rate is $1/T_0$. The excess bandwidth of $2W(1+\beta)$ is induced when employing a realistic root raised cosine (RRC) shaping filter having a roll-off factor $\beta > 0$. Hence, the achievable spectral efficiency of Nyquist signaling based on an RRC shaping filter becomes $(1+\beta)$-times lower than that of an idealistic rectangular shaping filter ($\beta = 0$). To overcome this limitation, the concept of faster-than-Nyquist (FTN) signaling has been explored for more than 50 years [1]–[6]. In FTN signaling, a symbol interval is set lower than that of Nyquist signaling, i.e., $T = \tau T_0$, where τ ($0 < \tau \leq 1$) represents a symbol packing ratio. Thus, the symbol rate of FTN signaling is higher than the Nyquist signaling counterpart, which is, naturally, achieved at the cost of the detrimental ISI effects. It has been proved that under the assumption of employing an RRC shaping filter, FTN signaling achieves a higher capacity than Nyquist signaling owing to the full exploitation of the excess bandwidth [7], [8]. As shown in the previous FTN studies [4]–[6], the concept of FTN signaling is applicable to a variety of communication scenarios, such as optical communications [9], visible

light communications [10], and digital video broadcast [11], in addition to typical microwave wireless communications. Similar to the above-mentioned single-carrier FTN signaling, the concept of multicarrier FTN (MFTN) signaling, which non-orthogonally packs information symbols in the time and/or frequency domain, has been studied [12]–[17]. In [18], [19], the practical hardware implementation issues of MFTN signaling were discussed, showing the hardware feasibility of channel-coded MFTN signaling employing the iterative soft decoders.

To efficiently demodulate ISI-contaminated FTN symbols, several time-domain (TD) receivers have been developed [20]–[23]. In [20], the TD trellis-based iterative decoding algorithm was first developed. In [21], the TD equalizer based on the Bahl, Cocke, Jelinek, and Raviv (BCJR) algorithm was presented. Also, Prlja and Anderson in [22] conceived the reduced-state M-algorithm-based BCJR (M-BCJR) algorithm to further reduce the decoding complexity. Moreover, in [23], the modified M-BCJR algorithm was proposed for the sake of striking a flexible balance between the detection performance and complexity. However, in the above-mentioned TD trellis-based detectors, the computational complexity significantly increases upon increasing the effective tap length and the constellation size, which becomes prohibitively high, especially in a realistic frequency-selective fading channel.

By contrast, low-complexity frequency-domain (FD) FTN receivers have been developed [24]–[27]. In [24], the single-carrier FD equalization (FDE) algorithm with the aid of cyclic prefix (CP) was first applied to FTN signaling, where the FD weights were derived based on the minimum-mean-square-error (MMSE) criterion. Owing to the efficient fast Fourier transform (FFT)-based implementation, practical low-complexity detection was achieved even in a highly dispersive frequency-selective fading channel. Moreover, in [25], the hard-decision MMSE-FDE algorithm in [24] was extended to its soft-decision (SoD) counterpart to support iterative detection. In [26], [27], the low-complexity FDE algorithm, capable of joint channel estimation and data detection, was presented for FTN signaling in a frequency-selective fading channel. In [28], the TD and FD receivers for FTN signaling were compared.

In contrast to the above-mentioned unprecoded FTN signaling [7], [29]–[33], precoded FTN signaling relying on the matrix factorization was proposed [8], [34]–[36]. In [8], the capacity of FTN signaling was derived based on the eigenvalue decomposition (EVD) of an FTN-induced ISI matrix, showing that the capacity of EVD-precoded FTN signaling without power allocation is identical to that of unprecoded FTN signaling in [7]. Furthermore, optimal power allocation was introduced to EVD-precoded FTN signaling [34], [37], which achieves a higher capacity than unprecoded FTN signaling and classic Nyquist signaling when employing the RRC shaping filter having $\beta > 0$ for each scheme [6], [36], [37]. Also, the capacity of EVD-precoded FTN signaling with optimal power allocation is maximized when $\tau = 1/(1+\beta)$, which achieves the spectral efficiency equal to that of Nyquist signaling employing an idealistic rectangular shaping filter ($\beta = 0$) [6], [36], [37].[1] This implies that despite the use of a realistic RRC shaping filter ($\beta > 0$), having the excess bandwidth, the Shannon capacity, i.e., that of Nyquist signaling employing an idealistic rectangular shaping filter ($\beta = 0$), is achievable in EVD-precoded FTN signaling with optimal power allocation. Furthermore, in [36], EVD-precoded FTN signaling with optimal power allocation designed for an AWGN channel [34] was extended to that supporting a frequency-selective fading channel, and the associated information rate was derived.[2] However, the computational complexity of the EVD-precoded FTN signaling scheme [36] is as prohibitively high as $\mathcal{O}(N^3)$, which is imposed by the EVD of an $(N \times N)$-sized equivalent channel matrix, where N represents the size of block transmission.

Against this background, the novel contributions of this paper are as follows.[3]

- We propose novel reduced-complexity FFT-spread multicarrier FTN (MFTN) signaling with power allocation for a frequency-selective fading channel. At the transmitter, each power-amplified information symbol is spread over an entire block by the IFFT-based precoding matrix, and hence the resultant transmit signal becomes a multicarrier signal. At the receiver, the received MFTN signal is decomposed into N parallel substreams by the FFT matrix. Owing to the low-complexity FFT-based implementation, the computational complexity order of the proposed MFTN transmitter and receiver is as low as $\mathcal{O}(N \log_2 N)$ per block while attaining good bit error ratio (BER) performance close to the optimal counterpart of [36].
- More specifically, the ISI matrix and the correlated noise covariance matrix, which are specific to received FTN signals, are approximated by circulant matrices to reduce the computational complexity imposed by our transceiver. This allows us to decompose the received signal into N independent parallel substreams with the aid of FFT-based factorization, hence enabling simplified symbol-by-symbol demodulation. Furthermore, the approximated achievable information rate of the proposed scheme is derived, which is then used to optimize power allocation coefficients.

1. Note that optimal power allocation of EVD-precoded FTN signaling [34] is implementable without elaborate symbol truncation only for $1/(1+\beta) \leq \tau \leq 1$ [6], [36], [37].

2. EVD-precoded FTN signaling with optimal power allocation [34], [37] is directly applicable to a frequency-flat fading channel [36].

3. The preliminary study of the scheme proposed in this paper was presented in [38]. However, [38] does not provide detailed performance investigations, including comparisons of the detection complexity, the peak-to-average-power ratio, and the power spectral density, while this paper does.

- We provide our performance results of BER, peak-to-average-power ratio (PAPR), and power spectral density (PSD) for the proposed MFTN signaling scheme with power allocation. It is demonstrated that the proposed MFTN scheme achieves the BER performance close to that of the conventional EVD-precoded FTN signaling counterpart [36], which is highly complex but optimal in terms of an information rate. The proposed scheme exhibits a higher PAPR while exhibiting a better BER performance than the open-loop unprecoded single-carrier FTN signaling and the conventional OFDM signaling ($\tau = 1$) counterparts, both having low complexity similar to the proposed scheme. Our PSD analysis reveals that the performance benefits of the proposed MFTN scheme are achieved without causing any significant bandwidth broadening.

The remainder of this paper is organized as follows. In Section II, we introduce the general system model of precoded FTN signaling in a frequency-selective fading channel while reviewing conventional EVD-precoded FTN signaling with optimal power allocation of [36]. In Section III, we propose the novel reduced-complexity FFT-spread MFTN signaling with power allocation. In Section IV, our numerical results of the BER, PAPR, and PSD of the proposed scheme are shown. Finally, this paper is concluded in Section V.

II. SYSTEM MODEL OF PRECODED FTN SIGNALING IN FREQUENCY-SELECTIVE FADING CHANNEL

A. GENERAL LINEARLY-PRECODED FTN SIGNALING

In this section, we introduce the general system model of linearly-precoded FTN signaling in a frequency-selective fading channel and then review the conventional EVD-precoded FTN signaling with optimal power allocation [36]. At the transmitter, information bits are modulated onto N-length complex-valued symbols $\mathbf{s} = [s_0, \ldots, s_{N-1}]^T \in \mathbb{C}^N$, where $\mathbb{E}[|s_k|^2] = \sigma_s^2$ $(k = 0, \ldots, N-1)$, and $\mathbb{E}[\cdot]$ is the expectation operation. Moreover, the modulated symbols $\mathbf{s}$ are precoded by a complex-valued matrix $\mathbf{P} \in \mathbb{C}^{N\times N}$ as follows:

$$\mathbf{x} = \mathbf{P}\mathbf{s} \in \mathbb{C}^N. \tag{1}$$

The precoded symbols $\mathbf{x}$ are passed through an RRC shaping filter $h(t)$ having the roll-off factor β with the symbol interval $T = \tau T_0$ to generate the transmit baseband FTN signal of

$$x(t) = \sum_n x_n h(t - nT). \tag{2}$$

Assuming an L-tap frequency-selective fading channel having the channel coefficients h_l $(l = 0, \ldots, L-1)$, the received signal after passing through the matched filter $h^*(-t)$ is represented by

$$y(t) = \sum_{l=0}^{L-1} \sum_n h_l x_n g(t - (l+n)T) + \eta(t), \tag{3}$$

where

$$g(t) = \int_{-\infty}^{\infty} h(\zeta) h^*(t-\zeta) d\zeta \tag{4}$$

$$\eta(t) = \int_{-\infty}^{\infty} n(\zeta) h^*(t-\zeta) d\zeta, \tag{5}$$

and $n(t)$ is a complex-valued Gaussian random process with the power spectral density of N_0. By sampling $y(t)$ at $t = kT$ $(k = 0, \ldots, N-1)$, the received sample block is obtained as

$$\mathbf{y} = \big[y(0), y(T), \ldots, y((N-1)T)\big] \in \mathbb{C}^N \tag{6}$$

$$= \mathbf{G}_{\mathrm{h}}\mathbf{x} + \boldsymbol{\eta}, \tag{7}$$

where $\mathbf{G}_{\mathrm{h}}$ represents the ISI matrix, including the effects of ISI induced by FTN signaling and the frequency-selective channel, whose kth-row and mth-column entry is given by

$$\mathbf{G}_{\mathrm{h}}(k, m) = \sum_{l=0}^{L-1} h_l g(kT - (m+l)T). \tag{8}$$

Moreover, $\boldsymbol{\eta} = [\eta(0), \eta(T), \ldots, \eta((N-1)T)]^T$ denotes the noise components, having an FTN-specific correlated covariance matrix of $\mathbb{E}[\boldsymbol{\eta}\boldsymbol{\eta}^H] = N_0\mathbf{G}$ [7], where $\mathbf{G} \in \mathbb{R}^{N\times N}$ has a Toeplitz structure, and its first column and first row are given by $[g(0), g(T), \ldots, g((N-1)T)]^T$ and $[g(0), g(-T), \ldots, g(-(N-1)T)]$, respectively. Note that in this paper, we consider a single block transmission, and the effects of inter-block interference (IBI) are ignored for the sake of simplicity.

With the aid of EVD, $\mathbf{G}$ is factorized into $\mathbf{G} = \mathbf{V}\boldsymbol{\Lambda}\mathbf{V}^T$ [8], where $\mathbf{V}$ is an orthogonal matrix, while $\boldsymbol{\Lambda}$ is a diagonal matrix having the descending-order eigenvalues $\lambda_0 \geq \cdots \geq \lambda_{N-1}$.[4]

Then, the average transmit energy of $x(t)$ is calculated as [36]

$$E = \mathbb{E}\left[\int_{-\infty}^{\infty} |x(t)|^2 dt\right] \tag{9}$$

$$= \mathbb{E}\left[\sum_k \sum_m x_k x_m^* g((k-m)T)\right] \tag{10}$$

$$= \mathbb{E}\left[\mathbf{x}^H\mathbf{G}\mathbf{x}\right] \tag{11}$$

$$= \mathbb{E}\left[\mathbf{s}^H\mathbf{P}^H\mathbf{G}\mathbf{P}\mathbf{s}\right]. \tag{12}$$

Let the precoding matrix $\mathbf{P}$ be $\mathbf{P} = \mathbf{I}_N$, where $\mathbf{I}_N$ represents the $(N \times N)$-sized identity matrix, and then the average transmit energy is given by [36]

$$E = N\sigma_s^2. \tag{13}$$

To maintain the transmit energy per block to be unchanged regardless of $\mathbf{P}$, the energy constraint of $E = N\sigma_s^2$ is imposed.

4. For finite N, all the eigenvalues λ_k are positive real values, irrespective of τ and β [8]. For $N \to \infty$, a subset of λ_k converges to zero when $\tau < 1/(1+\beta)$ [8].

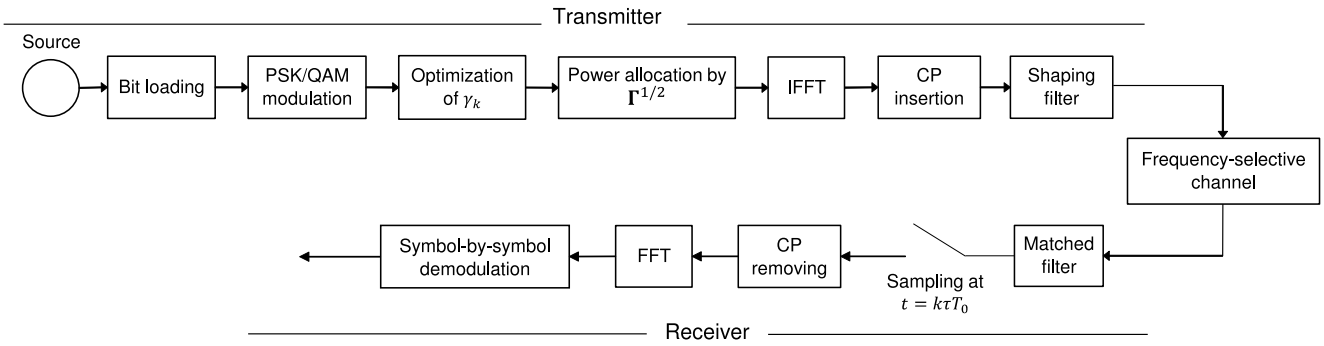

FIGURE 1. System model of the proposed reduced-complexity FFT-spread MFTN signaling scheme with power allocation for a channel-uncoded scenario.

As a part of demodulation, the received block (7) may be multiplied by a complex-valued weight matrix $\mathbf{W} \in \mathbb{C}^{N\times N}$ as follows:

$$\mathbf{y}_{\rm d} = \mathbf{W}\mathbf{y} \tag{14}$$
$$= \mathbf{W}\mathbf{G}_{\rm h}\mathbf{x} + \mathbf{W}\boldsymbol{\eta}. \tag{15}$$

B. CONVENTIONAL EVD-PRECODED FTN SIGNALING WITH OPTIMAL POWER ALLOCATION

In [36], EVD-precoded FTN signaling with optimal power allocation was proposed for a frequency-selective fading channel, where the precoding matrix $\mathbf{P}$ was designed to maximize the information rate. More specifically, based on EVD, the equivalent channel matrix $(\mathbf{\Lambda}^{-\frac{1}{2}}\mathbf{V}^T\mathbf{G}_{\rm h})^H\mathbf{\Lambda}^{-\frac{1}{2}}\mathbf{V}^T\mathbf{G}_{\rm h}$ is factorized into $\mathbf{U}\mathbf{\Xi}\mathbf{U}^H$, where $\mathbf{U}$ is a unitary matrix and $\mathbf{\Xi} = {\rm diag}[\xi_0, \ldots, \xi_{N-1}]$ is a diagonal matrix whose diagonal entries are given by the descending-order eigenvalues $\xi_0 \geq \cdots \geq \xi_{N-1}$.[5] Then, the precoding matrix is set to $\mathbf{P} = \mathbf{U}\mathbf{\Gamma}^{\frac{1}{2}}$, where $\mathbf{\Gamma} = {\rm diag}\{\gamma_0, \ldots, \gamma_{N-1}\}$ is a diagonal matrix, whose diagonal entries are optimized to maximize the achievable information rate based on the Lagrange multiplier method according to [36, (67)].

At the receiver, the weight matrix is set to $\mathbf{W} = \mathbf{U}^H(\mathbf{\Lambda}^{-\frac{1}{2}}\mathbf{V}^T\mathbf{G}_{\rm h})^H\mathbf{\Lambda}^{-\frac{1}{2}}\mathbf{V}^T$ that diagonalizes the received block while whitening the FTN-specific noise correlation matrix as seen in [36, (73), (77)], hence enabling the simplified symbol-by-symbol demodulation. However, the EVD of $(\mathbf{\Lambda}^{-\frac{1}{2}}\mathbf{V}^T\mathbf{G}_{\rm h})^H\mathbf{\Lambda}^{-\frac{1}{2}}\mathbf{V}^T\mathbf{G}_{\rm h}$ imposes prohibitively high computational complexity with the order of $\mathcal{O}(N^3)$ per block, which has to be updated every channel coherence time.

III. PROPOSED REDUCED-COMPLEXITY FFT-SPREAD MFTN SIGNALING WITH POWER ALLOCATION

In this section, we propose novel reduced-complexity FFT-spread MFTN signaling with power allocation for a frequency-selective fading channel. The block diagram of the proposed MFTN system is shown in Fig. 1. Similar to conventional single-carrier FTN signaling of [24], [26], the 2ν-length CP symbols are added to the precoded symbols $\mathbf{x}$ as follows:

$$\mathbf{x}_{\rm cp} = \left[x_{{\rm cp},0}, \ldots, x_{{\rm cp},N+2\nu-1}\right] \in \mathbb{C}^{N+2\nu} \tag{16}$$
$$= \mathbf{A}_{\rm cp}\mathbf{x} \tag{17}$$
$$= \mathbf{A}_{\rm cp}\mathbf{P}\mathbf{s}, \tag{18}$$

where

$$\mathbf{A}_{\rm cp} = \begin{bmatrix} \mathbf{0}_{2\nu\times(N-2\nu)} & \mathbf{I}_{2\nu} \\ \mathbf{I}_N & \end{bmatrix} \in \mathbb{R}^{(N+2\nu)\times N}, \tag{19}$$

and $\mathbf{0}_{2\nu\times(N-2\nu)}$ denotes the $(2\nu\times(N-2\nu))$-sized zero matrix. The CP-added FTN signal $x_{\rm cp}(t)$ is given by

$$x_{\rm cp}(t) = \sum_n x_{{\rm cp},n}h(t-nT), \tag{20}$$

At the receiver, the received signal after matched-filtering is represented by

$$y_{\rm cp}(t) = \sum_{l=0}^{L-1}\sum_n h_l x_{{\rm cp},n}g(t-(l+n)T) + \eta(t), \tag{21}$$

By removing the 2ν samples associated with CP from the received sample block $\mathbf{y} = [y_{\rm cp}(0), y_{\rm cp}(T), \ldots, y_{\rm cp}((N+2\nu-1)T)]^T$, the N-length received block are obtained as

$$\mathbf{r} = \left[r_0, \ldots, r_{N-1}\right]^T \in \mathbb{C}^N \tag{22}$$
$$= \left[y_{\rm cp}(\nu T), \ldots, y_{\rm cp}((N+\nu-1)T)\right]^T \tag{23}$$
$$= \mathbf{R}_{\rm cp}\mathbf{G}_{{\rm h},N+2\nu}\mathbf{A}_{\rm cp}\mathbf{x} + \boldsymbol{\eta}, \tag{24}$$

where

$$\mathbf{R}_{\rm cp} = \left[\mathbf{0}_{N\times\nu} \quad \mathbf{I}_N \quad \mathbf{0}_{N\times\nu}\right] \in \mathbb{R}^{N\times(N+2\nu)}. \tag{25}$$

while $\mathbf{G}_{{\rm h},N+2\nu}$ is the $((N+2\nu)\times(N+2\nu))$-sized ISI matrix whose kth-row and mth column entry is given by (8). Furthermore, by assuming the condition of

$$g(kT) = 0 \text{ for } |k| > \nu, \tag{26}$$

(24) is approximated by [24]–[26]

$$\mathbf{r} \simeq \mathbf{G}_{\rm c}\mathbf{x} + \boldsymbol{\eta}, \tag{27}$$

where the matrix $\mathbf{G}_{\rm c} \in \mathbb{C}^{N\times N}$ is the circulant matrix whose EVD is given by

$$\mathbf{G}_{\rm c} = \mathbf{Q}^H\mathbf{\Theta}\mathbf{Q}. \tag{28}$$

5. To accurately calculate $\mathbf{\Lambda}^{-\frac{1}{2}} = {\rm diag}[1/\sqrt{\lambda_0}, \ldots, 1/\sqrt{\lambda_{N-1}}]$, the minimum eigenvalues λ_{N-1} of $\mathbf{G}$ has to be higher than a specific value. To satisfy this condition, the symbol packing ratio τ has to be in the range of $1/(1+\beta) \leq \tau \leq 1$ [36].

Furthermore, $\mathbf{Q} \in \mathbb{C}^{N\times N}$ in (28) represents the normalized discrete Fourier transform (DFT) matrix whose kth-row and mth-column entry is given by $(1/\sqrt{N})\exp[-2\pi j(k-1)(m-1)/N]$. Additionally, $\mathbf{\Theta} = \mathrm{diag}\{\theta_0, \ldots, \theta_{N-1}\}$ is a diagonal matrix having the diagonal elements calculated by the FFT of the first column of $\mathbf{G}_\mathrm{c}$ [24], [26]. The modeling error induced due to the approximation of (26), i.e., the difference between the channel matrix $\mathbf{G}_\mathrm{t} = \mathbf{R}_\mathrm{cp}\mathbf{G}_{\mathrm{h},N+2\nu}\mathbf{A}_\mathrm{cp}$ and the approximated circulant matrix $\mathbf{G}_\mathrm{c}$, is investigated later in Section IV-A.

A. APPROXIMATED MUTUAL INFORMATION

Mutual information between the received block $\mathbf{r}$ and the transmit symbols $\mathbf{x}$ is formulated by

$$I(\mathbf{x};\mathbf{r}) = h_\mathrm{e}(\mathbf{r}) - h_\mathrm{e}(\mathbf{r}|\mathbf{x}) \tag{29}$$
$$= h_\mathrm{e}(\mathbf{r}) - h_\mathrm{e}(\boldsymbol{\eta}), \tag{30}$$

where $h_\mathrm{e}(\cdot)$ represents a differential entropy. The upper bounds of the differential entropies of $\mathbf{r}$ and $\boldsymbol{\eta}$ are given by [39]

$$h_\mathrm{e}(\mathbf{r}) \le \log_2\Big((\pi e)^N \Big|\mathbb{E}[\mathbf{r}\mathbf{r}^H]\Big|_\mathrm{det}\Big) \tag{31}$$
$$h_\mathrm{e}(\boldsymbol{\eta}) = \log_2\Big((\pi e)^N \Big|\mathbb{E}[\boldsymbol{\eta}\boldsymbol{\eta}^H]\Big|_\mathrm{det}\Big), \tag{32}$$

where $|\cdot|_\mathrm{det}$ denotes the determinant operation. For an instantaneous fading channel, the covariance matrix of the received block is approximately given by

$$\mathbb{E}\Big[\mathbf{r}\mathbf{r}^H\Big] \simeq \mathbb{E}\Big[(\mathbf{G}_\mathrm{c}\mathbf{x}+\boldsymbol{\eta})(\mathbf{G}_\mathrm{c}\mathbf{x}+\boldsymbol{\eta})^H\Big] \tag{33}$$
$$= \mathbf{G}_\mathrm{c}\mathbb{E}\Big[\mathbf{x}\mathbf{x}^H\Big]\mathbf{G}_\mathrm{c}^H + \mathbb{E}\Big[\boldsymbol{\eta}\boldsymbol{\eta}^H\Big] \tag{34}$$
$$= \mathbf{G}_\mathrm{c}\mathbf{R}_x\mathbf{G}_\mathrm{c}^H + N_0\mathbf{G}, \tag{35}$$

where we have $\mathbf{R}_x = \mathbb{E}[\mathbf{x}\mathbf{x}^H]$.

As shown in [40], for the limit of $N \to \infty$, a banded Toeplitz matrix $\mathbf{T} \in \mathbb{C}^{N\times N}$, whose first column and first row are given by $[t_0, t_1, \ldots, t_m, 0, \ldots, 0]^T$ and $[t_0, t_{-1}, \ldots, t_{-m}, 0, \ldots, 0]$, respectively, is asymptotically equivalent to a circulant matrix $\mathbf{C} \in \mathbb{C}^{N\times N}$, having the first column of $[t_0, t_1, \ldots, t_m, 0, \ldots, 0, t_{-m}, \ldots, t_{-1}]^T$. Hence, by assuming sufficiently large N and (26), the noise matrix $\mathbf{G}$, having the Toeplitz structure, is approximated by a circulant matrix whose first column is given by $\mathbf{g} = [g(0), g(T), \ldots, g(mT), 0, \ldots, 0, g(-mT), \ldots, g(-T)]^T$ ($0 \le m \le \lceil N/2-1\rceil$). In this paper, we assume the relationship of $m = \lceil N/2-1\rceil$. This allows us to factorize $\mathbf{G}$ based on the FFT as follows:

$$\mathbf{G} \simeq \mathbf{Q}^H\mathbf{\Psi}\mathbf{Q}, \tag{36}$$

where we have $\mathbf{\Psi} = \mathrm{diag}[\psi_0, \ldots, \psi_{N-1}] \in \mathbb{R}^{N\times N}$, whose diagonal entries are given by the FFT of $\mathbf{g}$.

Under the assumption of

$$1/(1+\beta) < \tau \le 1,$$

the upper bound of mutual information $I(\mathbf{x};\mathbf{r})$ is approximated by

$$I(\mathbf{x};\mathbf{r}) \le \log_2 \frac{(\pi e)^N\big|\mathbb{E}\big[\mathbf{r}\mathbf{r}^H\big]\big|_\mathrm{det}}{(\pi e)^N\big|\mathbb{E}\big[\boldsymbol{\eta}\boldsymbol{\eta}^H\big]\big|_\mathrm{det}} \tag{37}$$
$$\simeq \log_2 \frac{\big|\mathbf{G}_\mathrm{c}\mathbf{R}_x\mathbf{G}_\mathrm{c}^H + N_0\mathbf{G}\big|_\mathrm{det}}{|N_0\mathbf{G}|_\mathrm{det}} \tag{38}$$
$$= \log_2\left|\mathbf{I}_N + \frac{1}{N_0}\mathbf{G}_\mathrm{c}\mathbf{R}_x\mathbf{G}_\mathrm{c}^H\mathbf{G}^{-1}\right|_\mathrm{det} \tag{39}$$
$$\simeq \log_2\left|\mathbf{I}_N + \frac{1}{N_0}\mathbf{G}_\mathrm{c}\mathbf{R}_x\mathbf{G}_\mathrm{c}^H\mathbf{Q}^H\mathbf{\Psi}^{-1}\mathbf{Q}\right|_\mathrm{det} \tag{40}$$
$$= \log_2\left|\mathbf{I}_N + \frac{1}{N_0}\mathbf{Q}^H\mathbf{\Theta}\mathbf{Q}\mathbf{R}_x\mathbf{Q}^H\mathbf{\Theta}^H\mathbf{\Psi}^{-1}\mathbf{Q}\right|_\mathrm{det} \tag{41}$$
$$= \log_2\left|\mathbf{I}_N + \frac{1}{N_0}\mathbf{\Psi}^{-\frac{1}{2}}\mathbf{\Theta}\mathbf{Q}\mathbf{R}_x\mathbf{Q}^H\mathbf{\Theta}^H\mathbf{\Psi}^{-\frac{1}{2}}\right|_\mathrm{det}, \tag{42}$$

where the relationships of $|\mathbf{A}|_\mathrm{det}^{-1} = |\mathbf{A}^{-1}|_\mathrm{det}$ and $|\mathbf{I}_N + \mathbf{A}\mathbf{B}|_\mathrm{det} = |\mathbf{I}_N + \mathbf{B}\mathbf{A}|_\mathrm{det}$ are exploited.

Then, according to Hadamard's inequality [39], [41], the upper bound of the approximated mutual information (42) is maximized when $\mathbf{\Psi}^{-\frac{1}{2}}\mathbf{\Theta}\mathbf{Q}\mathbf{R}_x\mathbf{Q}^H\mathbf{\Theta}^H\mathbf{\Psi}^{-\frac{1}{2}}$ is a diagonal matrix, i.e., when $\mathbf{Q}\mathbf{R}_x\mathbf{Q}^H$ is a diagonal matrix. By letting $\mathbf{\Gamma} = \mathrm{diag}[\gamma_0, \ldots, \gamma_{N-1}] \in \mathbb{R}^{N\times N}$ be a real-valued diagonal matrix, (42) is maximized when the following equality holds:

$$\mathbf{Q}\mathbf{R}_x\mathbf{Q}^H = \sigma_\mathrm{s}^2\mathbf{\Gamma} \tag{43}$$
$$\mathbf{R}_x = \sigma_\mathrm{s}^2\mathbf{Q}^H\mathbf{\Gamma}\mathbf{Q} \tag{44}$$
$$\Leftrightarrow \mathbf{x} = \mathbf{Q}^H\mathbf{\Gamma}^{\frac{1}{2}}\mathbf{s}, \tag{45}$$

where we assume $\mathbb{E}[\mathbf{s}\mathbf{s}^H] = \sigma_\mathrm{s}^2\mathbf{I}_N$. Hence, from (1) and (45), the precoding matrix to be optimized is rewritten by

$$\mathbf{P} = \mathbf{Q}^H\mathbf{\Gamma}^{\frac{1}{2}}. \tag{46}$$

As seen from (46), the IFFT is performed on the information symbols; hence, the resultant transmit signal is a multicarrier signal. By substituting (45) into (42), the upper bound of the approximated mutual information is maximized as follows:

$$I(\mathbf{x};\mathbf{y}) \le \log_2\left|\mathbf{I}_N + \frac{\sigma_\mathrm{s}^2}{N_0}\mathbf{\Psi}^{-\frac{1}{2}}\mathbf{\Theta}\mathbf{\Gamma}\mathbf{\Theta}^H\mathbf{\Psi}^{-\frac{1}{2}}\right|_\mathrm{det} \tag{47}$$
$$= \sum_{k=0}^{N-1}\log_2\left(1 + \frac{\sigma_\mathrm{s}^2}{N_0}\gamma_k\theta_k^2\psi_k^{-1}\right). \tag{48}$$

B. POWER ALLOCATION

The coefficients γ_k are calculated to maximize the r.h.s of (48) based on the Lagrange multiplier method. From (11) and (46), the transmit energy of the CP-added symbols $\mathbf{x}_\mathrm{cp} = \mathbf{A}_\mathrm{cp}\mathbf{Q}^H\mathbf{\Gamma}^{\frac{1}{2}}\mathbf{s}$ is calculated by

$$E = \mathbb{E}\Big[\mathbf{x}_\mathrm{cp}^H\mathbf{G}_{N+2\nu}\mathbf{x}_\mathrm{cp}\Big] \tag{49}$$
$$= \mathbb{E}\Big[\mathrm{tr}\Big\{\mathbf{x}_\mathrm{cp}^H\mathbf{G}_{N+2\nu}\mathbf{x}_\mathrm{cp}\Big\}\Big] \tag{50}$$
$$= \mathbb{E}\Big[\mathrm{tr}\Big\{\mathbf{G}_{N+2\nu}\mathbf{x}_\mathrm{cp}\mathbf{x}_\mathrm{cp}^H\Big\}\Big] \tag{51}$$

$$= \mathrm{tr}\left\{\mathbf{G}_{N+2\nu}\mathbf{A}_{\mathrm{cp}}\mathbf{Q}^H\mathbf{\Gamma}^{\frac{1}{2}}\mathbb{E}\left[\mathbf{s}\mathbf{s}^H\right]\mathbf{\Gamma}^{\frac{1}{2}}\mathbf{Q}\mathbf{A}_{\mathrm{cp}}^T\right\} \tag{52}$$

$$= \sigma_{\mathrm{s}}^2\mathrm{tr}\left\{\mathbf{G}_{N+2\nu}\mathbf{A}_{\mathrm{cp}}\mathbf{Q}^H\mathbf{\Gamma}\mathbf{Q}\mathbf{A}_{\mathrm{cp}}^T\right\} \tag{53}$$

$$= \sigma_{\mathrm{s}}^2\mathrm{tr}\left\{\mathbf{\Gamma}\mathbf{Q}\mathbf{A}_{\mathrm{cp}}^T\mathbf{G}_{N+2\nu}\mathbf{A}_{\mathrm{cp}}\mathbf{Q}^H\right\} \tag{54}$$

$$= \sigma_{\mathrm{s}}^2\mathrm{tr}\{\mathbf{\Gamma}\mathbf{\Phi}\} \tag{55}$$

$$= \sigma_{\mathrm{s}}^2\sum_{k=0}^{N-1}\gamma_k\phi_k, \tag{56}$$

where

$$\mathbf{\Phi} = \mathbf{Q}\mathbf{A}_{\mathrm{cp}}^T\mathbf{G}_{N+2\nu}\mathbf{A}_{\mathrm{cp}}\mathbf{Q}^H, \tag{57}$$

and $\mathbf{G}_{N+2\nu} \in \mathbb{R}^{(N+2\nu)\times(N+2\nu)}$ represents the Toeplitz matrix whose first row and first column are given by $[g(0), g(-T), \ldots, g(-(N+2\nu)T)]$ and $[g(0), g(T), \ldots, g((N+2\nu)T)]^T$, respectively. Moreover, ϕ_k represents the kth diagonal element of $\mathbf{\Phi}$,[6] and $\mathrm{tr}\{\cdot\}$ represents the trace operation. With (13) and (56), we arrive at the energy constraint of

$$\sum_{k=0}^{N-1}\gamma_k\phi_k = N, \tag{58}$$

With (48) and (58), the Lagrange function is formulated by

$$J = \sum_{k=0}^{N-1}\log_2\left(1+\frac{\sigma_{\mathrm{s}}^2}{N_0}\gamma_k\theta_k^2\psi_k^{-1}\right) - \alpha\left(\sum_{k=0}^{N-1}\gamma_k\phi_k - N\right), \tag{59}$$

where α is the Lagrange multiplier. To maximize (59), the following problem is solved [34]:

$$\frac{\partial J}{\partial \gamma_k} = 0, \text{ subject to } \gamma_k \geq 0. \tag{60}$$

Finally, the power allocation coefficients γ_k are given by

$$\gamma_k = \max\left(\frac{1}{\alpha\phi_k\ln 2} - \frac{\psi_k N_0}{\theta_k^2\sigma_s^2}, 0\right), \tag{61}$$

which is calculated in the same manner as the classic water-filling algorithm [36], [42].

C. DETECTION ALGORITHM

In this section, the detection algorithm of the proposed MFTN signaling scheme is presented. Let us set the weight matrix to $\mathbf{W} = \mathbf{Q}$, and then from (14) and (27), the approximated received block is rewritten by

$$\mathbf{r}_{\mathrm{d}} \simeq \mathbf{Q}\mathbf{G}_{\mathrm{c}}\mathbf{x} + \mathbf{Q}\boldsymbol{\eta} \tag{62}$$

$$= \mathbf{Q}\mathbf{Q}^H\mathbf{\Theta}\mathbf{Q}\mathbf{Q}^H\mathbf{\Gamma}^{\frac{1}{2}}\mathbf{s} + \boldsymbol{\eta}_{\mathrm{q}} \tag{63}$$

$$= \mathbf{\Theta}\mathbf{\Gamma}^{\frac{1}{2}}\mathbf{s} + \boldsymbol{\eta}_{\mathrm{q}}, \tag{64}$$

where $\boldsymbol{\eta}_{\mathrm{q}} = \mathbf{Q}\boldsymbol{\eta}$. The covariance matrix of the noise components $\boldsymbol{\eta}_{\mathrm{q}}$ is approximately calculated by

$$\mathbb{E}\left[\boldsymbol{\eta}_{\mathrm{q}}\boldsymbol{\eta}_{\mathrm{q}}^H\right] = \mathbf{Q}\mathbb{E}\left[\boldsymbol{\eta}\boldsymbol{\eta}^H\right]\mathbf{Q}^H \tag{65}$$

$$= N_0\mathbf{Q}\mathbf{G}\mathbf{Q}^H \tag{66}$$

$$\simeq N_0\mathbf{Q}\mathbf{Q}^H\mathbf{\Psi}\mathbf{Q}\mathbf{Q}^H \tag{67}$$

$$= N_0\mathbf{\Psi}. \tag{68}$$

As shown in (64) and (68), the received block and the noise correlation matrix are approximately diagonalized. This allows us to carry out efficient sub-optimal symbol-by-symbol demodulation while reducing the effects of the correlated noises.

D. IMPLEMENTABLE RANGE OF PACKING RATIO

As discussed in Section II-B, in conventional EVD-precoded FTN signaling [36], the packing ratio τ is limited in the range of $1/(1+\beta) \leq \tau \leq 1$ to avoid computing potential extremely-low eigenvalues of $\mathbf{G}$. In the proposed MFTN signaling, the matrix $\mathbf{G}$ is approximated by $\mathbf{Q}^H\mathbf{\Psi}\mathbf{Q}$, where the approximation may cause the ill-conditioned problem for around the boundary of $\tau = 1/(1+\beta)$. Our extensive simulations revealed that for $\tau = 1/(1+\beta)$, the approximated eigenvalues may be negative, depending on m. Hence, in this paper, we impose further limitation on the packing ratio τ, i.e., $1/(1+\beta)+\delta \leq \tau \leq 1$, to ensure all the positive eigenvalues, where $\delta \in \mathbb{R}$ is a predefined small positive value. In our simulations, δ was set as 0.02.

E. COMPUTATIONAL COMPLEXITY

Table 1 shows the computational complexity of the proposed MFTN transceiver, which is compared with conventional TD and FD FTN signaling transceivers of [22]–[24], [26], [27], [36]. More specifically, the computational complexity of the TD BCJR equalizer is given by $\mathcal{O}(NK^{L_{\mathrm{e}}})$, where K and L_{e} represent the modulation size and the effective ISI-tap length, respectively [23], [28]. Hence, the complexity of the BCJR equalizer grows exponentially with L_{e}. Furthermore, the computational complexity of the reduced-complexity M-BCJR equalizer [22] is $\mathcal{O}(NMK)$ [23], where M denotes the number of the most possible surviving paths at each trellis stage. While the complexity of the M-BCJR equalizer grows linearly with N, M, and K, M becomes significantly high in a long-tap frequency-selective fading channel, considered in this paper. Moreover, both the BCJR and M-BCJR equalizers are imposed by multiple recursions on the trellis and multiple filtering at the receiver, as detailed in [22], [23]. The modified M-BCJR equalizer [23] exhibits the moderate complexity between the BCJR and the M-BCJR equalizers, where L_{b} in Table 1 represents the number of symbols considered in the trellis search.

The MMSE-FDE-aided receiver [24], [26] and the FD generalized approximated message passing (GAMP) receiver [27] are efficiently implemented with the aid of the

6. Note that $\mathbf{\Phi}$ is calculated offline since the matrices $\mathbf{Q}$, $\mathbf{A}_{\mathrm{cp}}$, and $\mathbf{G}_{N+2\nu}$ do not include channel state information (CSI), hence known in advance of transmission.

TABLE 1. Comparison of computational complexity.

System	Computational complexity
BCJR equalizer	$\mathcal{O}(NK^{L_e})$
M-BCJR equalizer [22]	$\mathcal{O}(NMK)$
Modified M-BCJR equalizer [23]	$\mathcal{O}\left(NMK^{\frac{K^{L_b+1}-1}{K-1}}\right)$
Simplified M-BCJR equalizer [23]	$\mathcal{O}\left(N\left(\frac{K^{L_b+1}-1}{K-1}+(L_b+1)\times(MK-1)\right)\right)$
MMSE-FDE-aided receiver [24, 26]	$\mathcal{O}(N\log N)$
MMSE-FDE-aided receiver with SIC [25, 26]	$\mathcal{O}(N^2)$
FD-GAMP equalizer [27]	$\mathcal{O}(N\log N)$
EVD-precoded transceiver [36]	$\mathcal{O}(N^3)$
Proposed MFTN transceiver	$\mathcal{O}(N\log N)$

N-point FFT and IFFT. Hence, the associated computational complexity is as low as $\mathcal{O}(N\log N)$, which does not depend on the ISI-tap length and the constellation size. For more details about the number of the FFT and IFFT operations, refer to [27]. When applying a soft interference cancelation (SIC) at the MMSE-FDE-aided receiver for further improving the detection performance, the associated computational complexity becomes $\mathcal{O}(N^2)$.

The computational complexity imposed to calculate precoding and weighting matrices of EVD-precoded FTN signaling with optimal power allocation [36] is dominated by the online EVD calculations, which is the order of $\mathcal{O}(N^3)$. By contrast, in our proposed MFTN signaling with power allocation, the eigenvalues θ_k and ϕ_k are approximated by the FFT coefficients, while the multiplications of the precoding matrix $\mathbf{P}=\mathbf{Q}^H\mathbf{\Gamma}^{\frac{1}{2}}$ and the weighting matrix $\mathbf{W}=\mathbf{Q}$ are efficiently computed by the IFFT and FFT, respectively. Furthermore, the power allocation coefficients (61) are computed by the order of $\mathcal{O}(N)$. Thus, the computational complexity of the proposed MFTN transceiver is given by $\mathcal{O}(N\log N)$, similar to the FD single-carrier FTN signaling receivers [24], [26], [27].

IV. SIMULATION RESULTS

In this section, we provide the simulation results to investigate the modeling error, the BER, the PAPR, and the PSD of the proposed MFTN signaling scheme. The minimum symbol interval of the Nyquist criterion was normalized to $T_0=1/2W=1$. We considered the L-tap quasi-static frequency-selective Rayleigh block fading channel. The channel coefficients h_l were randomly generated according to the complex-valued Gaussian distribution of $\mathcal{CN}(0,1/L)$ per block. Moreover, we employed the block length of $N=1024$ throughout the simulations. Unless otherwise noted, the roll-off factor of $\beta=0.25$ was employed.

A. MODELING ERROR OF ISI MATRIX

Fig. 2 shows the modeling error $\mathbb{E}[\|\mathbf{G}_t-\mathbf{G}_c\|^2]$ induced due to our approximation of (26), where the packing ratio was varied from $\tau=0.98$ to 0.1 with the step of 0.02. Moreover, the CP length was given by $\nu=10$, 20, 30, 40, 50, 100, and 200. The delay spread was set to $L=20$ and $L=40$ in Figs. 2(a) and 2(b), respectively. The results of 1000 random channel realizations were averaged. As shown in Fig. 2, the modeling error decreased upon increasing the CP length ν. Also, the modeling error decreased upon increasing the packing ratio τ. Naturally, to maintain a similarly low level of modeling errors, the higher ν has to be set for the higher L. Therefore, the CP length ν has to be designed to ensure the modeling error is sufficiently low, depending on τ, β, and L [25].

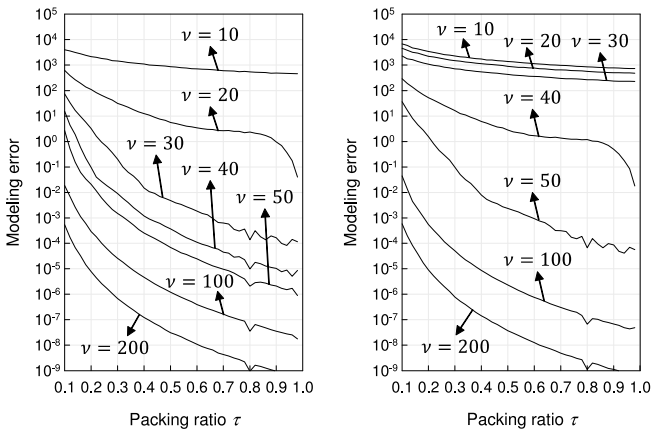

(a) $L=20$. (b) $L=40$.

FIGURE 2. Modeling errors $\mathbb{E}[\|\mathbf{G}_t-\mathbf{G}_c\|^2]$ of the proposed scheme, where the roll-off factor was fixed to $\beta=0.25$, while the packing ratio was varied from $\tau=0.98$ to 0.1 with the step of 0.02. The CP length was set to $\nu=10$, 20, 30, 40, 50, 100, and 200.

B. BER PERFORMANCE

In our BER calculations, we considered the three-stage serially-concatenated turbo coding architecture of [36], where the half-rate recursive systematic coding (RSC) encoder having the constraint length of 2 and octal generator polynomial (3, 2) was employed as the outer encoder, while the unity rate coding encoder was used as the inner encoder [43]. The number of outer decoding iteration and that of inner decoding iteration were set to 40 and 2, respectively [36]. Moreover, the target interleaver length was set to

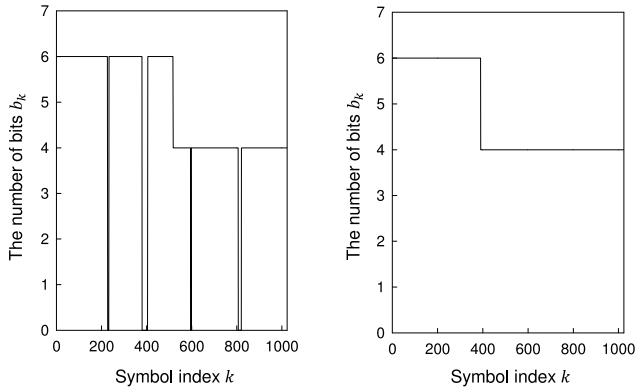

(a) With power allocation. (b) Without power allocation.

FIGURE 3. Snapshots of the bit-loading result for the proposed MFTN signaling (a) with power allocation and (b) without power allocation. We employed the system parameters of $\tau = 0.9$, $\beta = 0.25$, $N = 1024$, $L = 20$, and $\nu = 30$. The target transmission rate and SNR were set to $R_t = 2$ [bps/Hz] and 10 dB, respectively.

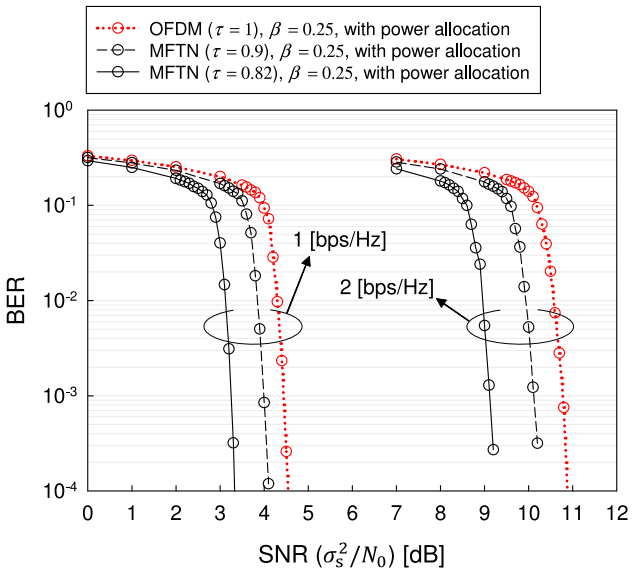

FIGURE 4. BER performance of the proposed MFTN signaling scheme with power allocation. The roll-off factor was fixed to $\beta = 0.25$, while the packing ratio was given by $\tau = 0.9$ and 0.82. The other system parameters were set to $N = 1024$, $L = 20$, and $\nu = 30$, and the target transmission rate was set to $R_t = 1$ and 2.

around 200000 bits.[7] Similar to conventional EVD-precoded FTN signaling [36], the log-likelihood ratio (LLR) of the received symbols is efficiently calculated since the equivalent channel matrix and the noise covariance matrix are approximately diagonalized. More specifically, the LLR of the kth received symbol $r_{d,k}$ is calculated based on the probability density function defined as follows:

$$p(r_{d,k}|s_k) = \frac{1}{\pi \phi_k N_0} \exp\left(-\frac{|r_{d,k} - \theta_k s_k|^2}{\phi_k N_0}\right). \tag{69}$$

The transmission rate of the proposed half-rate turbo-encoded FFT-spread FTN signaling system is given by

$$R_t = \frac{1}{2} \cdot \frac{1}{2W(1+\beta)} \cdot \frac{1}{(N+2\nu)\tau T_0} \cdot \sum_{k=0}^{N-1} b_k \text{ [bps/Hz]}, \tag{70}$$

where the coefficient $1/2$ represents the coding rate of the RSC code, and b_k denotes the number of bits assigned onto the kth symbol. The part of the symbols is deactivated when the associated power allocation coefficients are $\gamma_k = 0$ as a calculation result of (61). Hence, the number of bits b_k changes depending on CSI to maintain the target transmission rate, which is referred to as *bit-loading* in this paper.[8]

Fig. 3 shows the snapshots of bit-loading in the proposed scheme, where the power allocation was activated in Fig. 3(a) and deactivated in Fig. 3(b). The system parameters were set to $\tau = 0.9$, $L = 20$, and $\nu = 30$ while our optimization of (61) was carried out at the SNR of $\sigma_s^2/N_0 = 10$ dB. Moreover, the target transmission rate was set to $R_t = 2$, and hence we have $\sum_{k=0}^{N-1} b_k = 4878$. Observe in Fig. 3 that 64-QAM ($b_k = 6$) and 16-QAM ($b_k = 4$) were used for achieving the target transmission rate of $R_t = 2$. Moreover, subset symbols were deactivated in the proposed scheme with power allocation (Fig. 3(a)), while no symbols were deactivated in the proposed scheme without power allocation (Fig. 3(b)).

Fig. 4 shows the BERs of the proposed three-stage turbo-coded MFTN signaling scheme with power allocation, where the packing ratio was given by $\tau = 1$, 0.9 and 0.82, and other system parameters were given by $L = 20$, and $\nu = 30$. The target transmission rate was set to $R_t = 1$ and 2. For comparison, the BER curves of OFDM counterpart ($\tau = 1$) employing the same RRC shaping filter were plotted, where we set $2\nu = L = 20$ [44], [45]. Observe in Fig. 4 that the proposed MFTN scheme achieved better BER performance than its OFDM counterpart, and the proposed MFTN scheme with $\tau = 0.82$ achieved the best BER performance. More specifically, upon increasing the target transmission rate from $R_t = 1$ to 2, the performance advantage of the proposed scheme with $\tau = 0.82$ over the OFDM counterpart increased from 1.2 dB to 1.8 dB.

Fig. 5 shows the BERs of the proposed MFTN schemes with and without power allocation. For the proposed scheme without power allocation, we set $\gamma_k = 1$ ($k = 0, \ldots, N-1$) which dispenses with CSI for precoding, unlike the proposed scheme with power allocation. This implies that the proposed scheme without power allocation is the open-loop system, while the proposed scheme with power allocation is the closed-loop one. The packing ratio was set to $\tau = 0.9$, and other system parameters were the same as those used in

7. Similar to [36], multiple transmit blocks having the N symbols were concatenated by ignoring the detrimental IBI effects for simplicity.

8. In our simulations, binary phase-shift keying (BPSK) was used for all the activated symbols. Then, quadrature PSK (QPSK) was used to replace the BPSK-modulated symbols from the first activated symbol to the last one until the target transmission rate was achieved. The same operation was repeated using 16-point quadrature amplitude modulation (QAM), 64-QAM, 256-QAM, and 1024-QAM until the target transmission rate was achieved.

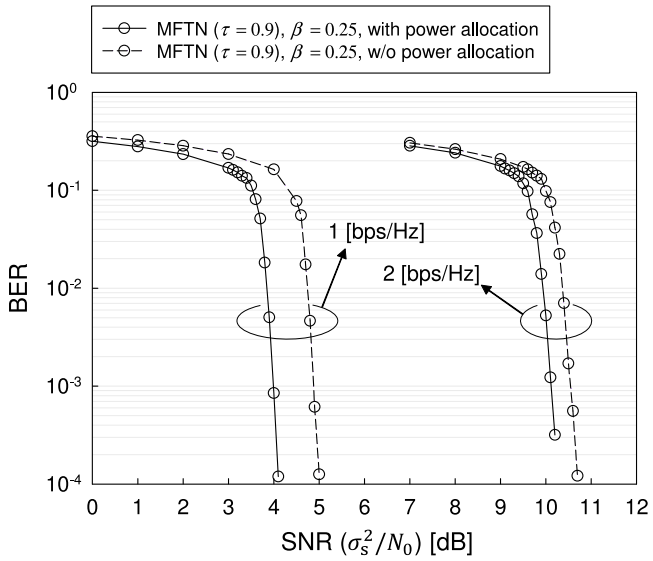

FIGURE 5. BER performance of the proposed MFTN signaling schemes with and without power allocation. The system parameters were set to $\beta = 0.25$, $\tau = 0.9$, $N = 1024$, $L = 20$, and $\nu = 30$. The target transmission rate was set to $R_t = 1$ and 2.

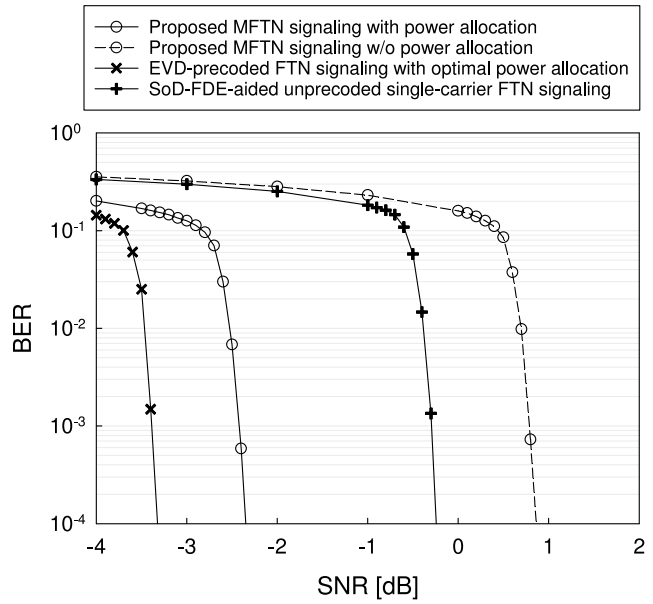

FIGURE 6. BER comparisons between the proposed MFTN signaling schemes with and without power allocation, the EVD-precoded FTN signaling scheme with optimal power allocation [36], and the open-loop SoD-FDE-aided unprecoded single-carrier FTN signaling scheme [26]. The system parameters were set to $\beta = 0.25$, $\tau = 0.82$, $N = 1024$, $L = 20$, $\nu = 30$, and $R_t = 0.461$.

Fig. 4. As shown in Fig. 5, our power allocation allows us to have the better BER performance, where the gap decreased upon increasing the transmission rate. More specifically, the gaps were 0.9 dB and 0.4 dB for $R_t = 1$ and 2, respectively.

Furthermore, Fig. 6 shows the BER comparisons between the proposed MFTN scheme with and without power allocation, the EVD-precoded FTN signaling scheme with optimal power allocation [36], and the open-loop SoD-FDE-aided unprecoded single-carrier FTN signaling scheme [26]. Note that the computational complexity in the proposed MFTN scheme is as low as $\mathcal{O}(N \log N)$, while that of the EVD-precoded FTN signaling scheme is $\mathcal{O}(N^3)$. The system parameters were set to $\tau = 0.82$, $L = 20$, and $\nu = 30$. The target transmission rate was set to $R_t = 0.461$ for each scheme. In Fig. 6, it was observed that the proposed MFTN scheme with power allocation outperformed two other open-loop schemes, i.e., SoD-FDE-aided unprecoded single-carrier FTN signaling scheme [26] and the proposed MFTN scheme without power allocation, where the associated performance gaps were 2.1 dB and 3.2 dB, respectively. Naturally, the EVD-precoded FTN signaling with optimal power allocation [36] exhibited the best performance owing to the optimality in terms of an achievable information rate, which is achieved at the cost of prohibitively high computational complexity. The penalty of the proposed scheme with power allocation over the EVD-precoded FTN signaling scheme with optimal power allocation [36] is imposed due to the circulant matrix approximation and the power penalty caused by the CP insertion. Note that a sufficiently long guard interval has to be added for the EVD-precoded FTN signaling benchmark [36] to eliminate the detrimental IBI effects, while it was ignored in our simulations.

C. PAPR PERFORMANCE

Next, we investigate the PAPR of the proposed MFTN signaling scheme, which is defined by

$$\mathrm{PAPR} = \frac{\max\left[|x(t)|^2\right]}{\mathbb{E}\left[|x(t)|^2\right]}, \tag{71}$$

where $\max[|x(t)|^2]$ represents the peak power of the continuous-time transmit signal $x(t)$, while $\mathbb{E}[|x(t)|^2]$ is the average power of $x(t)$. The transmit signal $x(t)$ was sampled with the step of $0.01T_0$ over the duration of $[-100T_0, (N + 2\nu)\tau T_0 + 100T_0]$.

Fig. 7 shows the complementary cumulative distribution function (CCDF) of the PAPR in the proposed scheme with power allocation, where the packing ratio was given by $\tau = 0.9$, 0.85, and 0.82, and other system parameters were set to $L = 20$, $\nu = 30$. The target transmission rate and the target SNR were set to $R_t = 2$ [bps/Hz] and 10 dB, respectively. The three-stage turbo encoding, as well as bit loading, was considered similar to Section IV-B. For comparisons, we plotted the PAPR of the OFDM counterpart ($\tau = 1$), employing the same RRC shaping filter. Observe in Fig. 7 that the proposed MFTN scheme with $\tau = 0.9$ and 0.85 exhibited lower PAPRs than the OFDM counterpart. This is because the constellation size of OFDM is higher than the proposed MFTN scheme to achieve the same target transmission rate, resulting in the use of more high-order QAM symbols. However, the PAPR of the proposed MFTN scheme with $\tau = 0.82$ was higher than that of the OFDM counterpart due to the effects of the non-orthogonal dense symbol packing. More specifically, the PAPR of MFTN signaling increases upon decreasing τ [46]. Hence, in Fig. 7,

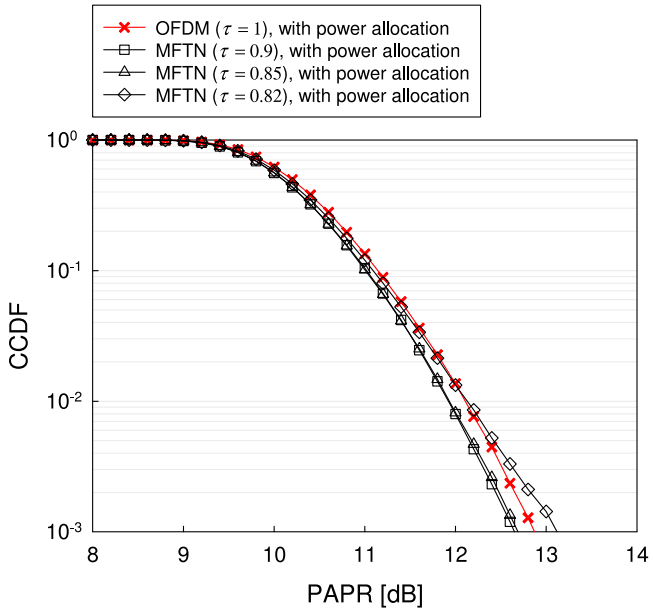

FIGURE 7. PAPRs of the proposed MFTN scheme with power allocation, where the packing ratio was set to $\tau = 0.9$, 0.85, and 0.82, and other system parameters were given by $\beta = 0.25$, $N = 1024$, $L = 20$, and $\nu = 30$. The target transmission rate and the target SNR were set to $R_t = 2$ and 10 dB, respectively.

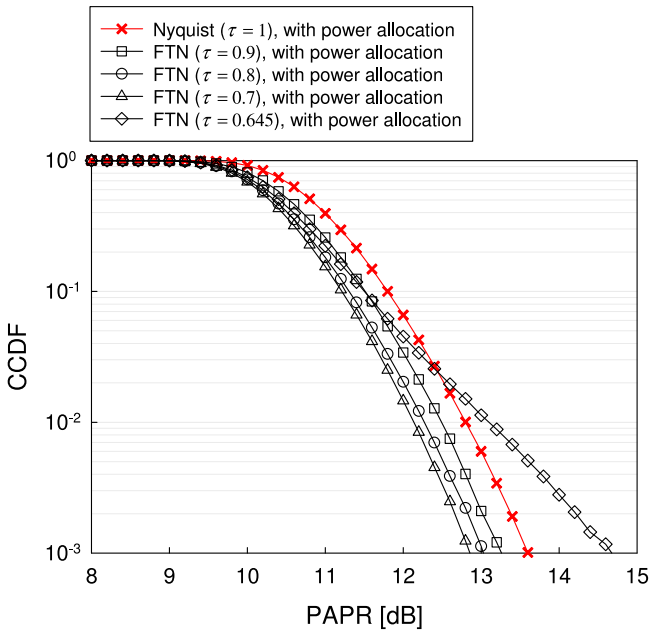

FIGURE 8. PAPRs of the proposed MFTN scheme with power allocation, where the roll-off factor was set to $\beta = 0.6$. The symbol packing ratio was set to $\tau = 0.9, 0.8, 0.7, 0.645 = 1/(1+\beta)+\delta$. The other system parameters were given by $N = 1024$, $L = 20$, $\nu = 30$, and $R_t = 2$. The target SNR was set to 10 dB.

the PAPR of FTN signaling associated with $\tau = 0.82$ was higher than that of the OFDM counterpart ($\tau = 1$) despite the use of lower-size QAM constellation.

Moreover, Fig. 8 depicts the PAPRs of the proposed MFTN scheme with power allocation, where the roll-off factor was set to $\beta = 0.6$. The symbol packing ratio was set to $\tau = 0.9, 0.8, 0.7, 0.645 = 1/(1+\beta)+\delta$. Observe in Fig. 8

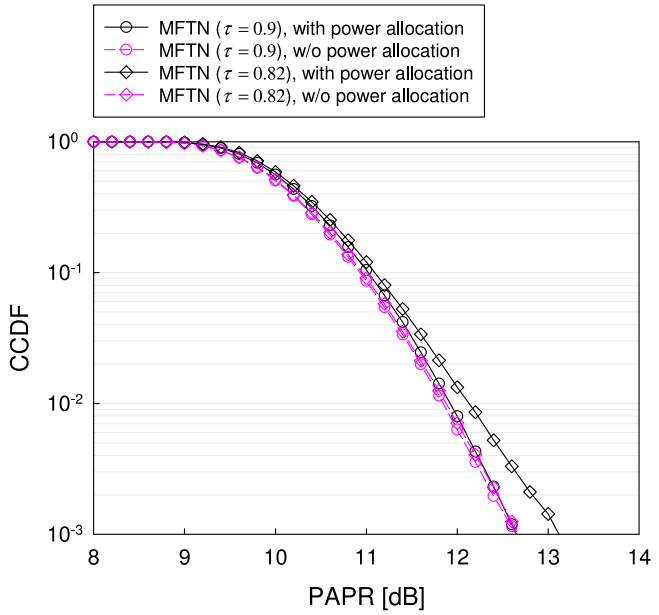

FIGURE 9. PAPRs of the proposed MFTN signaling schemes with and without power allocation, where the packing ratio was set to $\tau = 0.9$ and 0.82, and the other system parameters were given by $\beta = 0.25$, $N = 1024$, $L = 20$, and $\nu = 30$. The target transmission rate and the target SNR were set to $R_t = 2$ and 10 dB, respectively.

that the proposed MFTN scheme with $\tau \geq 0.7$ achieved the lower PAPR than OFDM counterpart. However, similar to Fig. 7, for the packing ratio of $\tau = 0.645$ which is close to the boundary $1/(1+\beta)$, the PAPR of the proposed scheme was higher than OFDM counterpart.

Fig. 9 shows the PAPRs of the proposed MFTN schemes with and without power allocation, where the packing ratio was set to $\tau = 0.9$ and 0.82, and the other system parameters were the same as those used in Fig. 7. In Fig. 9, the proposed scheme without power allocation exhibited a lower PAPR than that with power allocation for each τ scenario, where the gap increased upon decreasing τ.

Furthermore, Fig. 10 shows the PAPR comparisons between our proposed MFTN scheme with power allocation, the EVD-precoded FTN signaling scheme with optimal power allocation [36], and the open-loop unprecoded single-carrier FTN signaling scheme [26]. The packing ratio was fixed to $\tau = 0.9$, and the other system parameters were the same as those used in Fig. 7. As shown in Fig. 10, the PAPR of the unprecoded single-carrier FTN signaling was 3.4-dB lower than the proposed MFTN scheme at the CCDF of 10^{-3} due to the effects of IFFT-based precoding, while the proposed MFTN scheme exhibited slightly lower PAPRs than the EVD-precoded FTN signaling scheme.

D. PSD PERFORMANCE

Finally, we investigate the PSDs of the proposed MFTN scheme, where the transmit signal $x(t)$ was sampled with the step of $0.01T_0$ over the sufficiently-long duration of $[-100T_0, (N+2\nu)T_0+100T_0]$. Since the roll-off factor was fixed to $\beta = 0.25$, the one-sided bandwidth was $W(1+\beta) =$

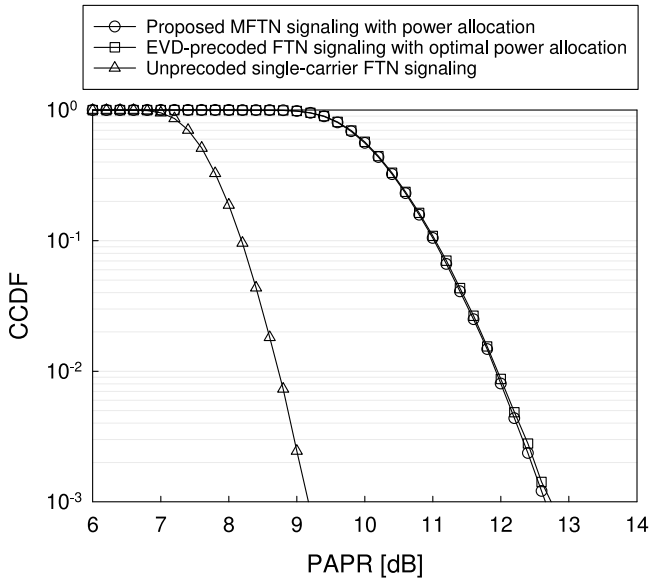

FIGURE 10. PAPR comparisons between the proposed MFTN scheme with power allocation, the EVD-precoded FTN signaling scheme with optimal power allocation [36], and open-loop unprecoded single-carrier FTN signaling scheme [26], where the system parameters were given by $\beta = 0.25$, $\tau = 0.9$, $N = 1024$, $L = 20$, and $\nu = 30$. The target transmission rate and the target SNR were set to $R_t = 2$ and 10 dB, respectively.

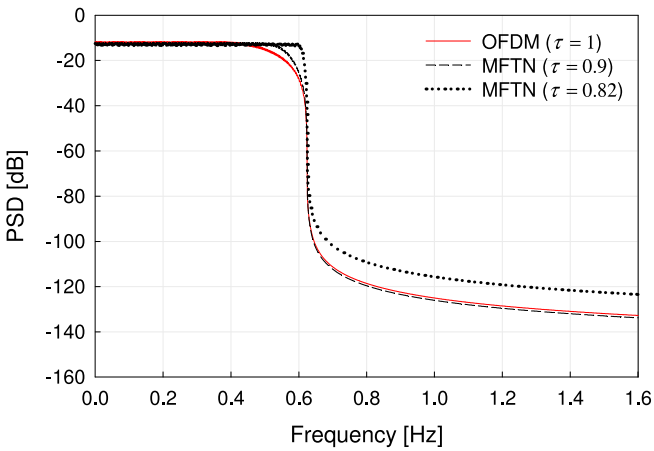

FIGURE 11. PSDs of the proposed MFTN signaling scheme with power allocation, where the packing ratio was set to $\tau = 0.9$ and 0.82, and the other system parameters were given by $\beta = 0.25$, $N = 1024$, $L = 20$, $\nu = 30$. The target SNR was set to 10 dB.

0.625. For simplicity, the BPSK modulation scheme was employed for all the scenarios.

Fig. 11 shows the PSDs of the proposed MFTN signaling scheme with power allocation, having $\tau = 0.9$ and 0.82, where the other system parameters were given by $L = 20$, and $\nu = 30$, while the target SNR was set to 10 dB. For comparisons, the PSD of the OFDM counterpart ($\tau = 1$) was also plotted. As shown in Fig. 11, the PSD of the proposed MFTN scheme exhibited the expected one-sided bandwidth of $W(1 + \beta) = 0.625$ in each τ scenario. Also, upon decreasing the packing ratio from $\tau = 0.9$ to 0.82 in the proposed scheme, the spectral side-lobe level increased. However, it remained sufficiently lower than the main-lobe level, indicating that the proposed MFTN signaling scheme with power allocation does not broaden the bandwidth.

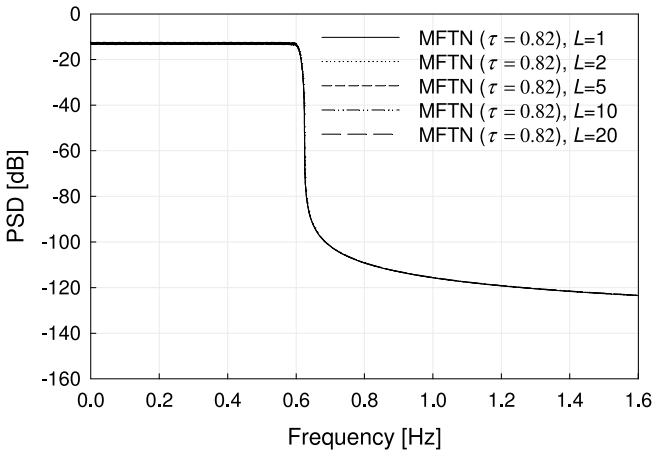

FIGURE 12. PSDs of the proposed MFTN signaling scheme with power allocation, where the system parameters were given by $\beta = 0.25$, $\tau = 0.82$, $N = 1024$, $\nu = 30$, while the delay spread was set to $L = 1$, 2, 5, 10, and 20. The target SNR was set to 10 dB.

Fig. 12 shows the PSDs of the proposed MFTN signaling scheme with power allocation, having $\tau = 0.82$, where the delay spread was given by $L = 1$, 2, 5, 10, and 20, and the other system parameters were the same as those used in Fig. 11. Observe in Fig. 12 that the PSD of the proposed MFTN scheme remained unchanged regardless of L without suffering from bandwidth broadening.

V. CONCLUSION

In this paper, we proposed the novel reduced-complexity FFT-spread MFTN signaling with power allocation for a frequency-selective fading channel. Under the circulant matrix approximation of the equivalent channel matrix and the noise correlation matrix, the approximated information rate of the proposed scheme was formulated. Then, the power allocation coefficients were optimized by maximizing the approximated information rate. Our simulation results demonstrated that the proposed closed-loop MFTN signaling scheme with power allocation achieved the BER performance close to the EVD-precoded FTN signaling bound, which is optimal in terms of an information rate while dramatically reducing the transceiver's computational complexity imposed by the calculations of precoding and weighting matrices. The conventional open-loop SoD-FDE-aided single-carrier FTN scheme with SIC outperformed the proposed open-loop MFTN scheme while the proposed MFTN scheme with power allocation exhibited a better BER performance. The performance benefits of the proposed scheme are achievable without suffering from bandwidth broadening.

REFERENCES

[1] B. Saltzberg, "Intersymbol interference error bounds with application to ideal bandlimited signaling," *IEEE Trans. Inf. Theory*, vol. 14, no. 4, pp. 563–568, Jul. 1968.

[2] J. Salz, "Optimum mean-square decision feedback equalization," *Bell Syst. Tech. J.*, vol. 52, no. 8, pp. 1341–1373, Oct. 1973.

[3] J. E. Mazo, "Faster-than-Nyquist signaling," *Bell Syst. Tech. J.*, vol. 54, no. 8, pp. 1451–1462, Oct. 1975.

[4] J. Anderson, F. Rusek, and V. Öwall, "Faster-than-Nyquist signaling," *Proc. IEEE*, vol. 101, no. 8, pp. 1817–1830, Aug. 2013.

[5] J. Fan, S. Guo, X. Zhou, Y. Ren, G. Y. Li, and X. Chen, "Faster-than-Nyquist signaling: An overview," *IEEE Access*, vol. 5, pp. 1925–1940, 2017.

[6] T. Ishihara, S. Sugiura, and L. Hanzo, "The evolution of faster-than-Nyquist signaling," *IEEE Access*, vol. 9, pp. 86535–86564, Jun. 2021.

[7] F. Rusek and J. B. Anderson, "Constrained capacities for faster-than-Nyquist signaling," *IEEE Trans. Inf. Theory*, vol. 55, no. 2, pp. 764–775, Feb. 2009.

[8] Y. J. D. Kim, "Properties of faster-than-Nyquist channel matrices and folded-spectrum, and their applications," in *Proc. IEEE Wireless Commun. Netw. Conf.*, Doha, Qatar, Apr. 2016, pp. 1–7.

[9] M. Jana, A. Medra, L. Lampe, and J. Mitra, "Pre-equalized faster-than-Nyquist transmission," *IEEE Trans. Commun.*, vol. 65, no. 10, pp. 4406–4418, Oct. 2017.

[10] Y. Zhu, W. Wang, and G. Xin, "Faster-than-Nyquist signal design for multiuser multicell indoor visible light communications," *IEEE Photon. J.*, vol. 8, no. 1, pp. 1–12, Feb. 2016.

[11] J. Lucciardi, P. Potier, G. Buscarlet, F. Barrami, and G. Mesnager, "Non-linearized amplifier and advanced mitigation techniques: DVB-S2X spectral efficiency improvement," in *Proc. IEEE Global Commun. Conf.*, Singapore, Dec. 2017, pp. 1–7.

[12] F. Rusek and J. B. Anderson, "Multistream faster than Nyquist signaling," *IEEE Trans. Commun.*, vol. 57, no. 5, pp. 1329–1340, May 2009.

[13] A. Barbieri, D. Fertonani, and G. Colavolpe, "Time-frequency packing for linear modulations: Spectral efficiency and practical detection schemes," *IEEE Trans. Commun.*, vol. 57, no. 10, pp. 2951–2959, Oct. 2009.

[14] D. Dasalukunte, F. Rusek, and V. Öwall, "Multicarrier faster-than-Nyquist transceivers: Hardware architecture and performance analysis," *IEEE Trans. Circuits Syst. I, Reg. Papers*, vol. 58, no. 4, pp. 827–838, Apr. 2011.

[15] M. Secondini *et al.*, "Optical time-frequency packing: Principles, design, implementation, and experimental demonstration," *J. Lightw. Technol.*, vol. 33, no. 17, pp. 3558–3570, Sep. 1, 2015.

[16] Y. Ma, F. Tian, N. Wu, B. Li, and X. Ma, "A low-complexity receiver for multicarrier faster-than-Nyquist signaling over frequency selective channels," *IEEE Commun. Lett.*, vol. 24, no. 1, pp. 81–85, Jan. 2020.

[17] Y. J. D. Kim and Y. Feng, "Capacity of multicarrier faster-than-Nyquist signaling," in *Proc. IEEE Int. Symp. Inf. Theory (ISIT)*, Los Angeles, CA, USA, Jun. 2020, pp. 2049–2054.

[18] D. Dasalukunte, F. Rusek, and V. Öwall, "Improved memory architecture for multicarrier faster-than-Nyquist iterative decoder," in *Proc. IEEE Comput. Soc. Annu. Symp. VLSI*, Chennai, India, Jul. 2011, pp. 296–300.

[19] D. Dasalukunte, F. Rusek, and V. Öwall, "An 0.8-mm^{2}9.6-mw iterative decoder for faster-than-Nyquist and orthogonal signaling multicarrier systems in 65-nm CMOS," *IEEE J. Solid-State Circuits*, vol. 48, no. 7, pp. 1680–1688, Jul. 2013.

[20] A. D. Liveris and C. N. Georghiades, "Exploiting faster-than-Nyquist signaling," *IEEE Trans. Commun.*, vol. 51, no. 9, pp. 1502–1511, Sep. 2003.

[21] A. Prlja, J. B. Anderson, and F. Rusek, "Receivers for faster-than-Nyquist signaling with and without turbo equalization," in *Proc. IEEE Int. Symp. Inf. Theory*, Jul. 2008, pp. 464–468.

[22] A. Prlja and J. B. Anderson, "Reduced-complexity receivers for strongly narrowband intersymbol interference introduced by faster-than-Nyquist signaling," *IEEE Trans. Commun.*, vol. 60, no. 9, pp. 2591–2601, Sep. 2012.

[23] S. Li, B. Bai, J. Zhou, P. Chen, and Z. Yu, "Reduced-complexity equalization for faster-than-Nyquist signaling: New methods based on Ungerboeck observation model," *IEEE Trans. Commun.*, vol. 66, no. 3, pp. 1190–1204, Mar. 2018.

[24] S. Sugiura, "Frequency-domain equalization of faster-than-Nyquist signaling," *IEEE Wireless Commun. Lett.*, vol. 2, no. 5, pp. 555–558, Oct. 2013.

[25] S. Sugiura and L. Hanzo, "Frequency-domain-equalization-aided iterative detection of faster-than-Nyquist signaling," *IEEE Trans. Veh. Technol.*, vol. 64, no. 5, pp. 2122–2128, May 2015.

[26] T. Ishihara and S. Sugiura, "Iterative frequency-domain joint channel estimation and data detection of faster-than-Nyquist signaling," *IEEE Trans. Wireless Commun.*, vol. 16, no. 9, pp. 6221–6231, Sep. 2017.

[27] Q. Shi, N. Wu, X. Ma, and H. Wang, "Frequency-domain joint channel estimation and decoding for faster-than-Nyquist signaling," *IEEE Trans. Commun.*, vol. 66, no. 2, pp. 781–795, Feb. 2018.

[28] S. Li, W. Yuan, J. Yuan, B. Bai, D. W. K. Ng, and L. Hanzo, "Time-domain vs. frequency-domain equalization for FTN signaling," *IEEE Trans. Veh. Technol.*, vol. 69, no. 8, pp. 9174–9179, Aug. 2020.

[29] Y. G. Yoo and J. H. Cho, "Asymptotic optimality of binary faster-than-Nyquist signaling," *IEEE Commun. Lett.*, vol. 14, no. 9, pp. 788–790, Sep. 2010.

[30] Y. J. D. Kim and J. Bajcsy, "Information rates of cyclostationary faster-than-Nyquist signaling," in *Proc. IEEE Can. Workshop Inf. Theory*, May 2011, pp. 1–4.

[31] M. Ganji, X. Zou, and H. Jafarkhani, "On the capacity of faster than Nyquist signaling," *IEEE Commun. Lett.*, vol. 24, no. 6, pp. 1197–1201, Jun. 2020.

[32] M. Yuhas, Y. Feng, and J. Bajcsy, "On the capacity of faster-than-Nyquist MIMO transmission with CSI at the receiver," in *Proc. IEEE Globecom Workshops*, San Diego, CA, USA, Dec. 2015, pp. 1–6.

[33] T. E. Bogale, L. B. Le, X. Wang, and L. Vandendorpe, "Multipath multiplexing for capacity enhancement in SIMO wireless systems," *IEEE Trans. Wireless Commun.*, vol. 16, no. 10, pp. 6895–6911, Oct. 2017.

[34] T. Ishihara and S. Sugiura, "SVD-precoded faster-than-Nyquist signaling with optimal and truncated power allocation," *IEEE Trans. Wireless Commun.*, vol. 18, no. 12, pp. 5909–5923, Dec. 2019.

[35] M. Mohammadkarimi, R. Schober, and V. W. S. Wong, "Channel coding rate for finite blocklength faster-than-Nyquist signaling," *IEEE Commun. Lett.*, vol. 25, no. 1, pp. 64–68, Jan. 2021.

[36] T. Ishihara and S. Sugiura, "Eigendecomposition-precoded faster-than-Nyquist signaling with optimal power allocation in frequency-selective fading channel," *IEEE Trans. Wireless Commun.*, vol. 21, no. 3, pp. 1681–1693, Mar. 2022.

[37] T. Ishihara and S. Sugiura. "Comments on and Corrections to 'SVD-Precoded Faster-Than-Nyquist Signaling With Optimal and Truncated Power Allocation.'" TechRxiv. 2021. [Online]. Available: https://doi.org/10.36227/techrxiv.14949681.v1

[38] T. Ishihara and S. Sugiura, "FFT-spread faster-than-Nyquist signaling in frequency-selective fading channel," in *Proc. IEEE Int. Conf. Commun.*, Seoul, South Korea, May 2022, pp. 1–6.

[39] T. M. Cover and J. A. Thomas, *Elements of Information Theory*. New York, NY, USA: Wiley, 1991.

[40] R. M. Gray, "Toeplitz and circulant matrices: A review," *Found. Trends Commun. Inf. Theory*, vol. 2, no. 3, pp. 155–239, 2006.

[41] A. Dembo, T. M. Cover, and J. A. Thomas, "Information theoretic inequalities," *IEEE Trans. Inf. Theory*, vol. 37, no. 6, pp. 1501–1518, Nov. 1991.

[42] A. Goldsmith, *Wireless Communications*. Cambridge, U.K.: Cambridge Univ. Press, 2005.

[43] D. Divsalar, S. Dolinar, and F. Pollara, "Serial concatenated trellis coded modulation with rate-1 inner code," in *Proc. IEEE Global Telecommun. Conf.*, vol. 2, San Francisco, CA, USA, Nov. 2000, pp. 777–782.

[44] N. Al-Dhahir, "Single-carrier frequency-domain equalization for space-time block-coded transmissions over frequency-selective fading channels," *IEEE Commun. Lett.*, vol. 5, no. 7, pp. 304–306, Jul. 2001.

[45] D. Falconer, S. L. Ariyavisitakul, A. Benyamin-Seeyar, and B. Eidson, "Frequency domain equalization for single-carrier broadband wireless systems," *IEEE Commun. Mag.*, vol. 40, no. 4, pp. 58–66, Apr. 2002.

[46] J. Lucciardi, N. Thomas, M. Boucheret, C. Poulliat, and G. Mesnager, "Trade-off between spectral efficiency increase and PAPR reduction when using FTN signaling: Impact of non linearities," in *Proc. IEEE Int. Conf. Commun.*, Kuala Lumpur, Malaysia, May 2016, pp. 1–7.

TAKUMI ISHIHARA (Member, IEEE) received the B.E., M.E., and Ph.D. degrees in computer and information sciences from the Tokyo University of Agriculture and Technology, Koganei, Japan, in 2016, 2017, and 2020, respectively. He is currently a Postdoctoral Research Fellow with the Institute of Industrial Science, The University of Tokyo, Tokyo, Japan. His research interest includes faster-than-Nyquist signaling. He was a recipient of the IEEE VTS Tokyo Chapter 2019 Young Researcher's Encouragement Award, the Yasujiro Niwa Outstanding Paper Award, in 2019, and the 33rd Telecom System Technology Award (Honorable Mention) from the Telecommunications Advancement Foundation, in 2018. He was certified as an Exemplary Reviewer of IEEE WIRELESS COMMUNICATIONS LETTERS in 2021.

SHINYA SUGIURA (Senior Member, IEEE) received the B.S. and M.S. degrees in aeronautics and astronautics from Kyoto University, Kyoto, Japan, in 2002 and 2004, respectively, and the Ph.D. degree in electronics and electrical engineering from the University of Southampton, Southampton, U.K., in 2010.

From 2004 to 2012, he was a Research Scientist with Toyota Central Research and Development Laboratories, Inc., Nagakute, Japan. From 2013 to 2018, he was an Associate Professor with the Department of Computer and Information Sciences, Tokyo University of Agriculture and Technology, Koganei, Japan. Since 2018, he has been an Associate Professor with the Institute of Industrial Science, The University of Tokyo, Tokyo, Japan, where he heads the Wireless Communications Research Group. In 2019, he was recognized as The University of Tokyo Excellent Young Researcher. His research has covered a range of areas in wireless communications, networking, signal processing, and antenna technology. He authored or coauthored over 80 IEEE journal papers.

Dr. Sugiura was a recipient of numerous awards, including the 18th JSPS Prize in 2022, the Fifth Yasuharu Suematsu Award in 2019, the Sixth RIEC Award from the Foundation for the Promotion of Electrical Communication in 2016, the Young Scientists' Prize by the Minister of Education, Culture, Sports, Science and Technology of Japan in 2016, the 14th Funai Information Technology Award (First Prize) from the Funai Foundation in 2015, the 28th Telecom System Technology Award from the Telecommunications Advancement Foundation in 2013, the Sixth IEEE Communications Society Asia-Pacific Outstanding Young Researcher Award in 2011, the 13th Ericsson Young Scientist Award in 2011, and the 2008 IEEE Antennas and Propagation Society Japan Chapter Young Engineer Award. He has served as an Editor for IEEE WIRELESS COMMUNICATIONS LETTERS since 2019 and as an Editor for *Scientific Reports* since 2021. He was certified as an Exemplary Editor for IEEE WIRELESS COMMUNICATIONS LETTERS in 2020, as an Exemplary Reviewer for IEEE COMMUNICATIONS LETTERS in 2013 and 2014, and IEEE TRANSACTIONS ON COMMUNICATIONS in 2018.